SYSTEMS BIOLOGY

Multimodal perception links cellular state to decision-making in single cells

Bernhard A. Kramer[1,2], Jacobo Sarabia del Castillo[1], Lucas Pelkmans[1]*

Individual cells make decisions that are adapted to their internal state and surroundings, but how cells can reliably do this remains unclear. To study the information processing capacity of human cells, we conducted multiplexed quantification of signaling responses and markers of the cellular state. Signaling nodes in a network displayed adaptive information processing, which led to heterogeneous growth factor responses and enabled nodes to capture partially nonredundant information about the cellular state. Collectively, as a multimodal percept this gives individual cells a large information processing capacity to accurately place growth factor concentration within the context of their cellular state and make cellular state–dependent decisions. Heterogeneity and complexity in signaling networks may have coevolved to enable specific and context-aware cellular decision-making in a multicellular setting.

Contextual decision-making by cells in a collective is a hallmark of multicellular systems (*1*–*4*). To achieve context-aware behavior, individual cells must integrate the input they receive from growth factors with complex information on their physicochemical state. Cells perceive this information through activation of intracellular signaling networks; however, individual signaling nodes in such networks are thought to have low capacity for processing information as a result of their highly variable growth factor responses in single cells (*5*–*7*). It thus remains largely unknown if and how individual cells can process a large amount of information in a contextual manner.

We explored the possibility that variable growth factor responses do not reflect a limited information processing capacity but instead represent adaptive information processing. In adaptive information processing the response of a signaling node in an individual cell is adapted to the physicochemical state of the cell and its surroundings (here collectively referred to as the cellular state), through mechanisms by which the cellular state controls the activities of signaling nodes (*8*, *9*). This implies that signaling responses not only capture information about the amount of growth factor a cell is exposed to but also—and perhaps primarily—obtain information about its cellular state. If the activation of different signaling nodes in a network is dependent on different properties of the cellular state then each node would carry partially nonredundant information. As a whole, the network could then generate a multimodal percept that captures a comprehensive picture of a cell's multicellular context and internal state, facilitating accurate and contextual decision-making.

[1]Department of Molecular Life Sciences, University of Zurich, Winterthurerstrasse 190, 8057 Zurich, Switzerland.
[2]Molecular Life Sciences PhD program, Life Science Zurich Graduate School, University of Zurich, Winterthurerstrasse 190, 8057 Zurich, Switzerland.
*Corresponding author. Email: lucas.pelkmans@mls.uzh.ch

Results

Multiplexed quantitative imaging of signaling and cellular state

To obtain multiple readouts of the cellular state in addition to signaling responses we applied 4i—a high-resolution multiplexing technology on the basis of iterative staining and elution of antibodies (*10*)—to human epithelial cells (184A1). After 4 days of growth, cells were deprived of serum and growth factors for 12 hours and subsequently exposed to five different concentrations of epidermal growth factor (EGF) for 5 min (Fig. 1A). After 30-plex 4i, cell segmentation, and quality control, the dataset contained ~8000 individual cells per replicate ($n = 3$) and condition (Fig. 1B and fig. S1, A to C), showing high technical and biological reproducibility (fig. S1, D to F). Images of cells reveal the highly heterogeneous nature of acute signaling responses as well as that of the cellular state (Fig. 1C). Quantifying the abundances of three signaling responses and three cellular state markers in every cell and comparing single-cell distributions of the five conditions revealed that although signaling responses typically display changing levels with increasing amounts of EGF in either a gradual or switch-like bimodal manner, their responses were highly heterogeneous between cells. This results in overlapping single-cell distributions between different doses of EGF (Fig. 1D and fig. S2, A and B). By contrast, cellular state markers did not show any change (Fig. 1D). A systematic assessment of all single-cell features quantified from the images revealed that ten signaling responses downstream of EGF displayed significant changes whereas 650 features of the cellular state did not change during a 5 min exposure to EGF (Fig. 1E). These features quantify or act as proxies of properties across multiple spatial scales such as relative cell positioning within a population, position in the cell cycle, and subcellular textures of organelles (Fig. 1F and fig. S2, C and D). Thus although the cellular state changes in response to EGF stimulation (*11*), this occurs at longer timescales. Inhibitors of signaling nodes abrogated signaling responses to EGF but did not change markers of the cellular state (fig. S2E). We can thus test whether the heterogeneity seen in acute EGF-induced signaling responses is linked to the preexisting heterogeneity in cellular states.

The preexisting cellular state landscape shapes signaling responses in single cells

A projection of the multidimensional cellular state space into a two-dimensional (2D) landscape (*12*) was largely continuous except for two parts that reflect G1 and G2 of the cell cycle (Fig. 1F and fig. S2, F and G). Signaling responses of single cells distribute in different patterns across this landscape [Fig. 2A (middle) and fig. S4A], which was accurately predicted by features of the cellular state (Fig. 2A and fig. S3). This required multiple features in different combinations for different signaling nodes (fig. S4, B to D). For instance, although local cell density was an important feature for most signaling responses, the abundance of Paxillin—a proxy for cell spreading—was particularly important for predicting levels of pS6 in single cells, the abundance of Sec13 was particularly important for predicting pERK, and the amount of nuclear Yap1 was important for predicting nuclear translocation of FoxO3a [Fig. 2A (middle) and fig. S4B]. Thus the cellular state has a specific multivariate effect on signaling responses in individual cells. It also predicts switch-like bimodal response properties (being either a low or high responder) with high accuracy, as shown by some signaling nodes at low doses of EGF (Fig. 2B, Fig. 1D, fig. S2B, and fig. S4E), and achieves high prediction accuracy across the full range of EGF doses tested (Fig. 2C, fig. S4F, and fig. S5). As a result, variation in signaling responses induced by different cellular states is typically larger than variation induced by different concentrations of EGF (Fig. 2, D and E).

Multimodal perception accurately decodes EGF concentration

The above suggests that the sensitivity of signaling nodes—quantified by the effective concentration of EGF at which a node is half-maximally activated (EC_{50})—is adapted to the cellular state. To study this, we defined 18 cellular state classes and compared their dose-response curves (Fig. 3A and fig. S6, A to E). This showed that, for instance, the EC_{50} of pERK differed by a factor of at least three between

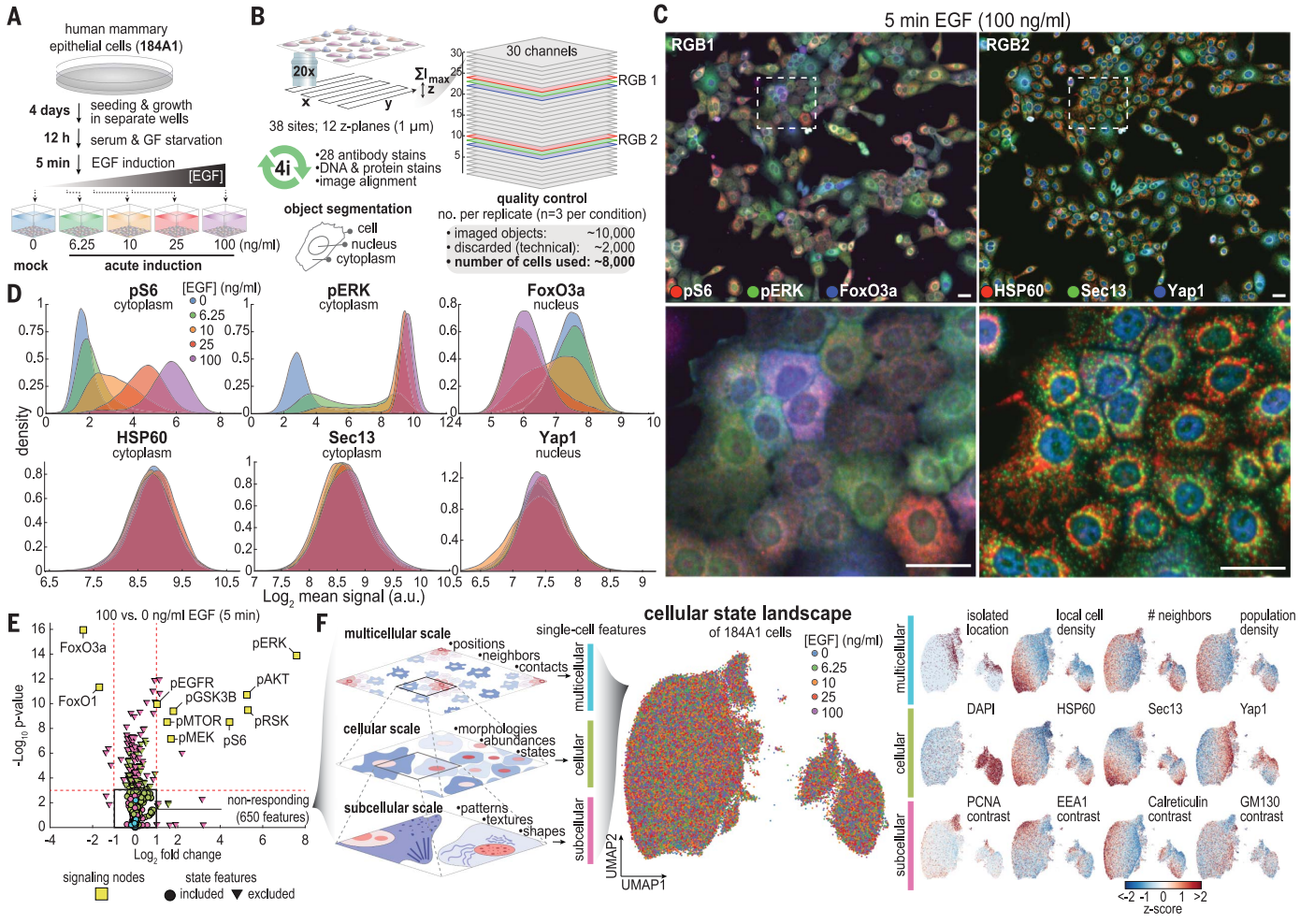

Fig. 1. Acute signaling responses and preexisting cellular states across spatial scales. (**A**) Experimental workflow. (**B**) 4i, imaging setup and quality control pipeline. (**C**) Two combinations of three channels of one imaging site (top) and zoom-in of cells (bottom). Scale bars: 7.5 µm. (**D**) Density distributions of mean intensities in either the cytoplasm or nucleus of six markers. (**E**) Systematic identification of features that change or do not change upon EGF treatment. *P* value was estimated with a two-tailed *t* test comparing replicates treated with 100 ng/ml to 0 ng/ml EGF. (**F**) Single-cell nonresponding features (143 principal components) define the cellular state space, projected using UMAP embedding. (Left) Schematic of features derived from multiple spatial scales. (Middle) Position of cells from each condition. (Right) Values from selected cellular state features.

cellular states (Fig. 3B), with class 2 cells (small cells grown in densely populated areas and having abundant early endosomes) showing a particularly high EC_{50} and class 15 cells (grown in sparsely populated regions and having nuclear Yap1) a low EC_{50}. Inferring single-cell EC_{50}s revealed that the sensitivity of each signaling node was adapted to the cellular state in distinct ways and for different ranges of EGF concentrations (Fig. 3C and fig. S6F).

To test whether signaling node–specific, cellular state–conditioned sensitivity to EGF could provide enough information to individual cells to perceive a wide range of EGF concentrations in a contextual manner, we quantified the amount of mutual information between the signaling responses of individual cells and the five doses of EGF they are exposed to (*13*). Perfect decoding ability would show mutual information of log2(5) or 2.3 bits. When cells were considered to use information from one node (unimodal perception) and it was assumed that their signaling was not conditioned to the cellular state (noncontextual), cells could only distinguish large differences between individual doses (Fig. 3D) and had little decoding capacity (0.7 bits) (Fig. 3E and fig. S7, A to C). When we considered that the cellular state affects the signaling response (contextual), smaller differences between individual doses could be distinguished and the decoding capacity of individual cells increased (1.2 bits). When cells were considered to use information from multiple nodes (multimodal perception) (*14*) they could approach perfect decoding (2.1 bits), but only when conditioning by the cellular state was considered (Fig. 3, D to E). Inhibitor experiments showed that a multimodal response was required to achieve the greatest accuracy. Inhibiting either MEK or AKT reduced the perception accuracy of EGF concentration and inhibiting both led to a stronger reduction (Fig. 3F and fig. S7, D to F). This indicates that multimodal perception could enable individual cells to accurately distinguish a range of EGF concentrations in a manner that is conditioned to the cellular state.

Multimodal perception comprehensively maps cellular state space

Conditioning by the cellular state implies that the multimodal response of an individual

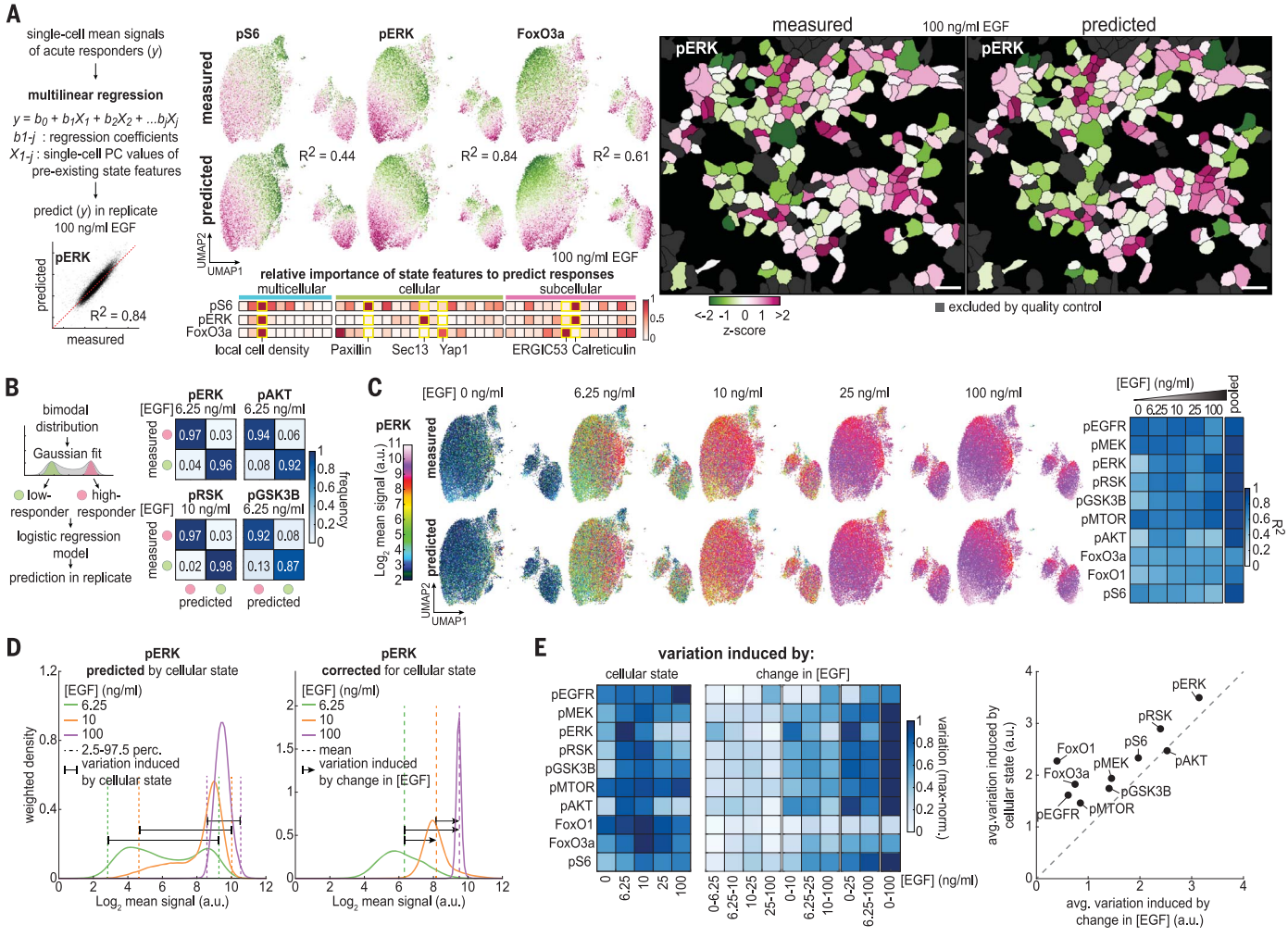

Fig. 2. Cellular state determines the heterogeneous signaling response. (**A**) (Left) Regression approach. (Upper middle) Measured and predicted levels of three signaling response markers. R^2, explained variance. (Lower middle) Dominance analysis of cellular state features in explaining signaling responses. Yellow boxes indicate specific examples. (Right) Side-by-side projection of measured and predicted levels of pERK. Scale bars: 15 μm. (**B**) (Left) Logistic regression. (Right) Confusion matrices for class predictions of bimodal responses. (**C**) (Left) Measured and predicted levels of pERK across all concentrations of EGF. (Right) R^2 for all signaling responses across all EGF concentrations. (**D**) Variation in signaling responses induced by the preexisting cellular state- and variation-induced EGF treatment. (Left) pERK at three EGF concentrations predicted by cellular state. (Right) pERK at three EGF concentrations corrected for variation in cellular state. (**E**) (Left) Quantification of cellular state- and EGF-induced variation as described in (D). (Right) Mean variation induced by all concentration changes in EGF (*x* axis) versus the mean variation induced by cellular state at all concentrations of EGF (*y* axis). Dashed line, $x = y$.

cell to EGF carries a considerable amount of information about the cellular state, especially if nodes in a network not only contain redundant but also unique information and can act in a synergistic manner (Fig. 4A). For instance, the cytoplasmic abundances of pERK and pMTOR in cells show a strong positive correlation, suggesting redundancy, which is observed to various degrees for all nodes in the network (Fig. 4A and fig. S8A). However, the amounts of pERK and pMTOR also scale with cellular state properties that are distinct when compared with the other as illustrated for Sec13 and HSP60 (Fig. 4A). This can be revealed by partial correlation analysis, indicating that the amounts of pERK scale with the abundance of Sec13 whereas the amounts of pMTOR scale with the abundance of HSP60, and can be appreciated in images of individual cells that differ in the abundance of one but not the other cellular state marker (Fig. 4A). To estimate the amount of information pERK and pMTOR carry about these cellular state properties and to decompose it into redundant (captured by either node), unique (captured by one node), and synergistic components (captured only by the combined response of both nodes), we employed partial information decomposition (PID) (*15*). pERK and pMTOR capture redundant but also unique information about Sec13 and HSP60 abundance, respectively (Fig. 4A, right bar graphs). For the latter, pERK and pMTOR also capture synergistic information.

We next applied this analysis to all tested nodes (Fig. 4, B and C, and fig. S8B), showing that each node displays some distinct scaling with various cellular state properties (Fig. 4B). Many of these effects have previously been reported such as (negative) pMEK scaling with local cell density (*16*), pAKT scaling with cell area (*8*), pRSK scaling with the

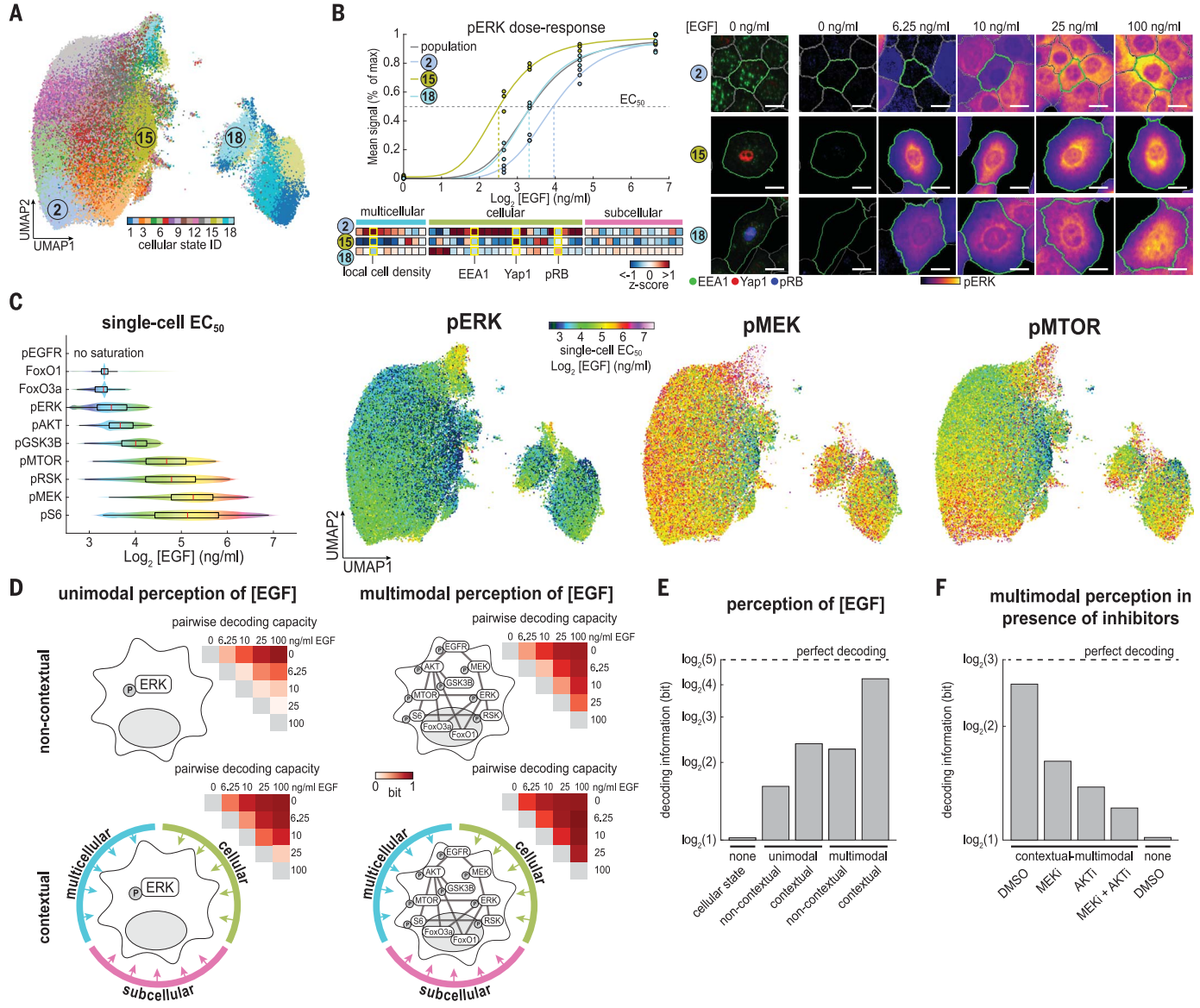

Fig. 3. Contextual multimodal perception of EGF concentration. (**A**) Cellular state classes (highest membership coefficient) from fuzzy clustering on the cellular state landscape. (**B**) (Left) dose-response curves of pERK for the whole population (gray) and for three cellular state classes. Dots, individual replicates. (Bottom) Values of cellular state features. Yellow boxes indicate examples. (Right) Cellular state markers and (left) pERK in representative cells of three state classes outlined in green. Scale bars: 2.5 μm. (**C**) Single-cell EC_{50} was calculated by combining measured responses with predicted (regression). (Left) Single-cell EC_{50} values for each signaling node. (Right) EC_{50} values on cellular state landscape for three signaling nodes. (**D**) Capacity to distinguish two EGF concentrations based on different perception modes. Decoding capacity is calculated from predicted and true EGF exposure labels. (**E**) Decoding capacity of EGF concentrations for different perception modes for all concentrations simultaneously. (**F**) Decoding capacity of contextual multimodal perception in the presence of different inhibitors.

transcriptional state of cells (pPolII) (*17*), pGSK3b scaling with the abundance of late endosomes (VPS35) (*18*), and pEGFR scaling with the abundance of Paxillin (*19*) (Fig. 4B). Only by analyzing these multiple connections between signaling responses and cellular state properties collectively in the same cells and across many cells can we observe that nodes capture not only redundant but also unique and synergistic information about the cellular state (Fig. 4C and fig. S9). To test whether this information propagates through the network, we used inhibitors. The redundant information about cellular state features between upstream (pAKT and pERK) and downstream nodes (respectively nuclear FoxO3a and pS6) was reduced upon inhibition of the upstream node (Fig. 4D), whereas the unique information about the cellular state captured by the downstream node was not reduced and sometimes increased (fig. S8C). For instance, although nuclear depletion of FoxO3a was reduced when AKT was inhibited it was still heterogeneous and correlated more strongly with position in the cell cycle (fig. S8D). Thus, cellular state information can propagate through the network and nodes can integrate information from multiple sources depending on the activity of other nodes.

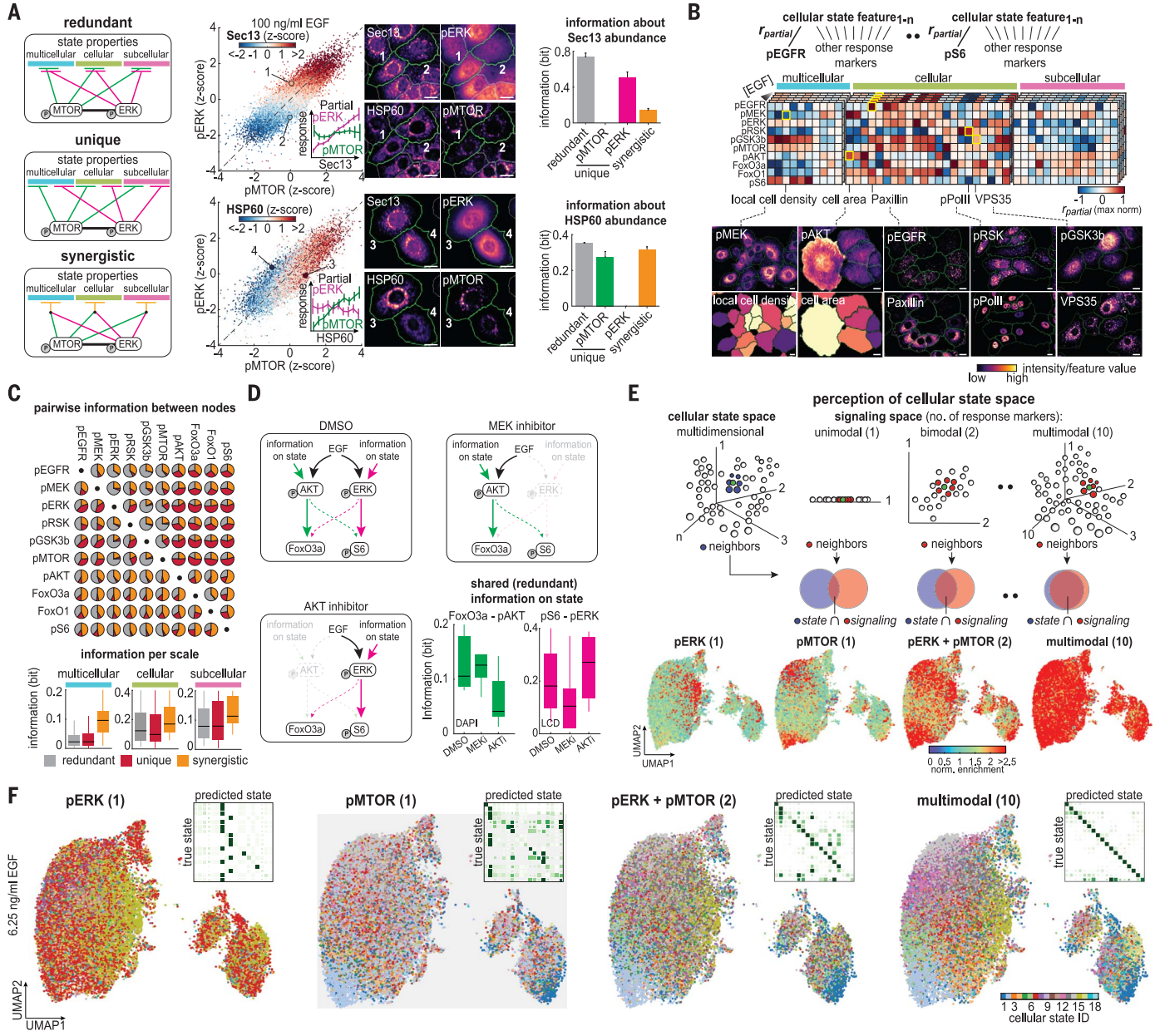

Fig 4. Multimodal perception captures the diversity of cellular states. (**A**) (Left) Encoding regimes of cellular state information by signaling nodes. (Middle left) Scatterplot of pMTOR and pERK abundances with Sec13 (top) or HSP60 (bottom) abundances visualized. (Inlets) Partial scaling of pERK and pMTOR with Sec13 and HSP60. (Middle right) Representative cells (green outlines) illustrating the partial scaling. Scale bars: 5 μm. (Right) Redundant, unique, and synergistic information on Sec13 and HSP60 encoded by pERK and pMTOR from PID. (**B**) (Top) Quantifying the unique scaling signaling nodes display with cellular state features. (Middle) Partial correlations (maximum normalized per signaling node) of each node with cellular state features. (Bottom) Representative cells illustrating the indicated scaling (yellow boxes). Scale bars: 2.5 μm. (**C**) (Top) Relative amount of redundant, unique, and synergistic information about the cellular state (averaged across all features) that signaling nodes encode (pairwise comparison). (Bottom) Encoding cellular state information as average across all pairwise combinations of signaling nodes. (**D**) Transfer of cellular state information from pAKT and pERK to FoxO3a and pS6 in presence of inhibitors and amount of redundant information on the indicated cellular state properties. (**E**) (Top) Calculating neighbor similarity between cellular state space and different signaling spaces. (Bottom) Similarity of cellular state space and different signaling neighborhoods. (**F**) Cellular state classes (as in Fig. 3A) predicted for each cell (logistic classifier) from indicated signaling spaces. (Inlets) Confusion matrices. Color indicates the fraction of cells assigned to a class. Square size indicates posterior probability of cells with that prediction.

To analyze whether collectively, as a multimodal percept, signaling nodes can comprehensively map cellular state space and inform an individual cell on its position in this space, we quantified the overlap between the statistical neighbors of an individual cell in cellular state space with its statistical neighbors in signaling space (Fig. 4E). Unimodal perception can only map neighborhoods within small regions of the cellular state space (Fig. 4E and fig. S10A) whereas a multimodal percept based on 10 nodes can map the neighborhood across the whole cellular state space (Fig. 4E and fig. S10B). The information gain in multimodal perception is particularly high for the first six nodes in the network (fig. S10C). Furthermore, only multimodal perception can accurately predict to which cellular state class an individual cell belongs for a large diversity of cellular states (Fig. 4F and fig. S10, D and E).

Multimodal perception links cellular state to decision-making

To test whether multimodal perception is used by cells to make context-aware decisions we exposed cells to longer EGF stimulation. To avoid problems resulting from the fact that

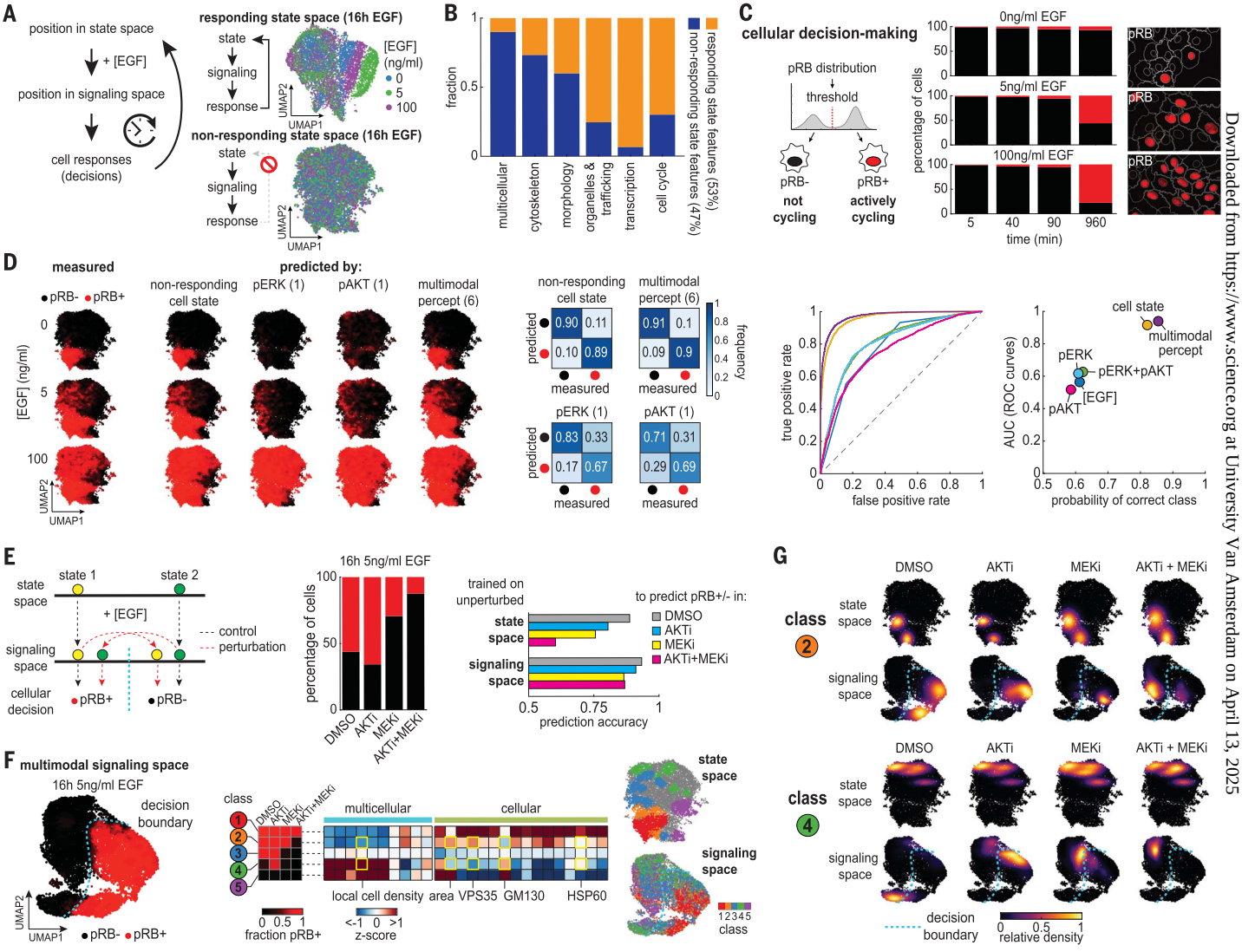

Fig. 5. Multimodal perception links cellular state to decision-making. (**A**) (Left) Position in cellular state space conditions signaling response. On long time scales, this changes the position in state space. (Top right) UMAP of the responding cellular state. (Bottom right) UMAP of the nonresponding cellular state. (**B**) Fractions of cellular state features related to properties and activities that change after 16 hours of EGF. (**C**) (Left) Classification of pRB status. (Middle) Fraction pRB status. (Right) Representative images. (**D**) (Left) Measured and predicted (logistic regression using indicated variables) pRB status on the cellular state landscape. Accuracy (middle), and ROC curves (left) of the classifier. (**E**) (Left) Perturbations that only affect position in signaling space and not in state space, changes the decision expected of distinct cellular states. (Middle) Fraction of pRB status with different inhibitors. (Right) Prediction accuracy of a logistic regression classifier trained on dimethyl sulfoxide (DMSO)–treated cells predicting pRB status in cells treated with inhibitors using the indicated spaces as variables. (**F**) (Left) pRB status visualized on a UMAP of the multimodal signaling space. Dashed blue line, decision boundary. (Middle left) Fraction of pRB status in different cellular state classes across inhibitors. (Middle right) Values of selected cellular state features. (Right) Cellular state class on UMAPs of state and signaling space. (**G**) Density of cellular state classes cells projected on both state and signaling space. Class 2 (top) and Class 4 (bottom).

some properties of the cellular state may change during longer stimulation times, we defined a nonresponding cellular state space (Fig. 5A and fig. S11A). This resulted in the exclusion of about half of all cellular state features and enrichment of features related to the transcriptional state and cell proliferation but also to cell morphology, the cytoskeleton, and membrane trafficking (Fig. 5B and fig. S11A). One of these is phosphorylated retinoblastoma protein (pRB), which is under the control of multiple signaling nodes (*11, 20*). RB is phosphorylated in actively proliferating cells and marks an EGF dose-dependent decision-making event to reenter the cell cycle (Fig. 5C). Projecting the status of individual cells as pRB-negative (pRB−) or pRB-positive (pRB+) after 16 hours of EGF induction on the cellular state landscape showed specific patterns across different doses of EGF, which were accurately predicted by using properties of the cellular state (Fig. 5D and fig. S11B). pRB status was also accurately predicted by the multimodal percept of single cells but less accurately by the responses of individual signaling nodes or their combination (Fig. 5D and fig. S11B). Thus, both the position in cellular state space as well as the position in multimodal signaling space allows for an accurate prediction of the response of single cells to reenter the cell cycle.

We next treated cells with inhibitors of AKT (AKTi) and MEK (MEKi). At low concentrations these inhibitors did not affect the positions of cells in cellular state space but did so in multimodal signaling space (fig. S11, C and D), both alone and in combination, resulting in altered fractions of pRB status (Fig. 5E). These altered responses were not accurately predicted by models based on the cellular state if trained on unperturbed cells but were accurately predicted by models based on the multimodal percept (Fig. 5E, right bar graph). Models based on the cellular state trained on perturbed cells were also accurate (fig. S11E). Thus, the position in multimodal signaling space couples cellular state to decision-making, which is altered by the inhibitors. To explore this we projected pRB status of both untreated and treated cells in the multimodal signaling landscape, revealing a sharp decision boundary (Fig. 5F). We then defined five classes of cells from cellular state space each with a distinct decision-making profile across perturbations. These classes occupy different regions in cellular state space and consequently different regions in multimodal signaling space (Fig. 5F). Although their positions in cellular state space remained the same during inhibitor treatment, their positions in multimodal signaling space changed, affecting the response of these cells (Fig. 5G and fig. S11F). For instance class 2 cells, which grew in regions of low local cell density and were large with abundant late endosomes, were located on the pRB+ side of the decision boundary (Fig. 5F). Individually inhibiting AKT or MEK affected their position in multimodal signaling space but did not result in crossing of the pRB decision boundary (Fig. 5G). Inhibiting both AKT and MEK resulted in altered pRB status (Fig. 5G). Thus, cells in this state were only prevented from re-entering the cell cycle by inhibiting both AKT and MEK. By contrast class 4 cells, which grew in regions of high local cell density, were small and had relatively few endosomes but an abundant Golgi complex, and were located on the pRB− side of the decision boundary in the unperturbed condition (Fig. 5F). Although all treatments affected their position in multimodal signaling space they only became pRB+ upon inhibition of AKT (Fig. 5G). Thus, cells in this state remained nonproliferative upon EGF stimulation but became aberrantly proliferative upon AKT inhibition.

Discussion

We have shown that the heterogeneity in acute signaling responses of individual cells contains partially nonredundant information about the cellular state that influences the growth factor response. The cellular state has a stronger effect on these responses than changes in growth factor concentration and thus represents an important source of information to predict these responses. Collectively, as a multimodal percept this enables individual cells to accurately sense a range of growth factor concentrations and to integrate this with their cellular state to make cellular state–dependent decisions. The cellular state is thus at least as relevant as growth factor concentration in determining cellular responses. This suggests that one purpose of cellular structures in controlling the activation of signaling nodes (*8, 9*) is to inject information about the cellular state into the decision-making process. It may also help explain why signaling responses are heterogeneous and signaling networks have a certain complexity. Although the redundant elements in network complexity can counteract uncertainty in individual responses (*5*) the nonredundant and synergistic elements can enable adaptive responses of multiple nodes to act as a multimodal percept that captures a large amount of information about the cellular state. This suggests that a collective of cells repeatedly generates the same spectrum of single-cell responses through generating the same landscape of cellular states. This may be important during development in which spatial effects and self-organization could drive the robust formation of such landscapes, providing the appropriate context for morphogens to induce a range of cellular decisions even in the absence of well-defined gradients (*21, 22*). That the cellular state determines the heterogeneous response of signaling nodes to clinically tested inhibitors resulting in different and sometimes unwanted state-dependent decisions may also be relevant for the treatment of diseases such as cancer (*23*).

REFERENCES AND NOTES

1. T. Hashimshony, M. Feder, M. Levin, B. K. Hall, I. Yanai, *Nature* **519**, 219–222 (2015).
2. D. Serra *et al.*, *Nature* **569**, 66–72 (2019).
3. J. Yao, A. Pilko, R. Wollman, *Mol. Syst. Biol.* **12**, 894 (2016).
4. B. Snijder *et al.*, *Nature* **461**, 520–523 (2009).
5. R. Cheong, A. Rhee, C. J. Wang, I. Nemenman, A. Levchenko, *Science* **334**, 354–358 (2011).
6. S. Sampattavanich *et al.*, *Cell Syst.* **6**, 664–678.e9 (2018).
7. J. Selimkhanov *et al.*, *Science* **346**, 1370–1373 (2014).
8. M. Frechin *et al.*, *Nature* **523**, 88–91 (2015).
9. A. V. Vieira, C. Lamaze, S. L. Schmid, *Science* **274**, 2086–2089 (1996).
10. G. Gut, M. D. Herrmann, L. Pelkmans, *Science* **361**, eaar7042 (2018).
11. D. T. Worster *et al.*, *Sci. Signal.* **5**, ra19 (2012)
12. E. Becht *et al.*, *Nat. Biotechnol.* **37**, 38–44 (2018).
13. S. A. Cepeda-Humerez, J. Ruess, G. Tkačik, *PLOS Comput. Biol.* **15**, e1007290 (2019).
14. S. Zmigrod, B. Hommel, *Multisens. Res.* **26**, 143–157 (2013).
15. N. M. Timme, C. Lapish, *eNeuro* **5**, ENEURO.0052-18.2018 (2018).
16. S. Ito, N. Kioka, K. Ueda, *Biosci. Biotechnol. Biochem.* **83**, 463–471 (2019).
17. T. S. K. Eisinger-Mathason *et al.*, *Mol. Cell* **31**, 722–736 (2008).
18. V. F. Taelman *et al.*, *Cell* **143**, 1136–1148 (2010).
19. M. Saxena *et al.*, *Nat. Mater.* **16**, 775–781 (2017).
20. J. Y. Chen, J. R. Lin, K. A. Cimprich, T. Meyer, *Mol. Cell* **45**, 196–209 (2012).
21. B. Ewen-Campen, T. Comyn, E. Vogt, N. Perrimon, *Cell Rep.* **32**, 108121 (2020).
22. C. Gerri *et al.*, *Nature* **587**, 443–447 (2020).
23. M. Fallahi-Sichani, S. Honarnejad, L. M. Heiser, J. W. Gray, P. K. Sorger, *Nat. Chem. Biol.* **9**, 708–714 (2013).
24. B. Kramer, Data_Multimodal_Perception_Cells, Version 2, figshare (2022).

ACKNOWLEDGMENTS

We thank all members of the Pelkmans lab for discussions. We further thank P. Liberali, W. Kramer, R. Klemm, and D. Gilmour for critical suggestions to improve the manuscript. **Funding:** Swiss National Science Foundation grant 310030_192622 (to L.P.); the European Research Council advanced grant CROSSINGSCALES-885579 (to L.P.); the Chan Zuckerberg Initiative grant CZF2019-002440 (to L.P.); and the University of Zurich (to L.P.). **Author contributions:** Conceptualization: B.A.K. and L.P. Methodology: B.A.K. and L.P. Experiments: B.A.K. and J.S.C. Data analysis: B.A.K. Visualization: B.A.K. and L.P. Writing: B.A.K. and L.P. **Competing interests:** L.P. has filed a patent on the 4i technology. **Data and materials availability:** All scripts and code used, and detailed description of the data can be accessed at https://github.com/hlardirian/Multimodal_Signaling. All data used can be downloaded at (*24*) **License information:** Copyright © 2022 the authors, some rights reserved; exclusive licensee American Association for the Advancement of Science. No claim to original US government works. https://www.sciencemag.org/about/science-licenses-journal-article-reuse

SUPPLEMENTARY MATERIALS

science.org/doi/10.1126/science.abf4062
Materials and Methods
Figs. S1 to S11
Tables S1 to S5
References (*25–27*)

View/request a protocol for this paper from *Bio-protocol*.

Submitted 23 October 2020; resubmitted 3 September 2021
Accepted 1 July 2022
10.1126/science.abf4062